Realtime wavefront sensing in a SPIM microscope, and active aberration tracking

Taylor, Jonathan, Saunter, Christopher, Bourgenot, Cyril, Girkin, John, Love, Gordon

Jonathan M. Taylor, Christopher D. Saunter, Cyril Bourgenot, John M. Girkin, Gordon D. Love, "Realtime wavefront sensing in a SPIM microscope, and active aberration tracking," Proc. SPIE 9335, Adaptive Optics and Wavefront Control for Biological Systems, 93350A (31 March 2015); doi: 10.1117/12.2080061

SPIE.

Event: SPIE BiOS, 2015, San Francisco, California, United States

Invited Paper

Realtime wavefront sensing in a SPIM microscope, and active aberration tracking

Jonathan M. Taylor[a], Christopher D. Saunter[b], Cyril Bourgenot[b], John M. Girkin[b], Gordon D. Love[b]

[a]School of Physics and Astronomy, Glasgow University, UK;
[b]Department of Physics, Durham University, UK

ABSTRACT

Adaptive optics (AO) can potentially allow high resolution imaging deep inside living tissue, mitigating against the loss of resolution due to aberrations caused by overlying tissue. Closed-loop AO correction is particularly attractive for moving tissue and spatially varying aberrations, but this requires direct wavefront sensing, which in turn requires suitable "guide stars" for use as wavefront references. We present a novel method for generating an orthogonally illuminated guide star suitable for direct wavefront sensing in a wide range of fluorescent biological structures, along with results demonstrating its use for measuring time-varying aberrations, *in vivo*.

1. INTRODUCTION

The use of adaptive optics (AO) has been shown to enhance optical microscopy, especially when imaging some distance inside a specimen.[1–3] However a substantial proportion of work to date has focused on the use of so-called sensorless adaptive optics,[4] in which the most appropriate wavefront correction is determined by guided iteration through a series of trial corrections applied to a deformable mirror in the pupil plane of the imaging system. This technique has been shown to be highly effective in correcting time-independent aberrations, but its iterative nature means that it is not well suited to correcting time-varying aberrations (although it is possible to phase-lock the sensorless AO to a cyclic pattern such as a regularly-beating heart[5]).

An alternative approach well-established in astronomical AO is the use of "guide stars".[6] A bright star can be treated as a reference wavefront source (flat wavefronts from a distant point source, prior to entering the atmosphere), and the aberrations induced by passage through the atmosphere can be measured – for example by using a Shack-Hartmann wavefront sensor. If a suitably bright star is not available in the field of view, then an artificial laser guide star can be generated in the upper atmosphere through high power laser illumination. These direct wavefront sensing approaches are better suited to rapidly-changing aberrations, due to the snapshot nature of the wavefront measurement.

Attempts to follow a similar approach in microscope imaging face substantial challenges in generating a reference source that is sufficiently localized in all three dimensions and is bright enough to serve as a wavefront reference. One possible solution involves the introduction of fluorescent microbeads into the specimen to serve as a guide star.[7] A non-invasive alternative is the use of existing fluorescent protein labelling in the specimen, in cases where this takes the form of highly localized and well separated point structures.[8] The technique we report here uses a new geometry for laser illumination which allows the generation of a 3D-localized guide star in a wide range of fluorescently-labelled living tissues. Our technique is suitable for use on fluorescent structures including 1D linear structures (e.g. blood vessels) and 2D surface structures (e.g. heart muscle), as well as 3D punctate structures, thus offering considerably more flexibility in the range of samples on which wavefront sensing can be performed.

Correspondence email: jonathan.taylor@glasgow.ac.uk

Adaptive Optics and Wavefront Control for Biological Systems, edited by Thomas G. Bifano, Joel Kubby, Sylvain Gigan, Proc. of SPIE Vol. 9335, 93350A · © 2015 SPIE
CCC code: 1605-7422/15/$18 · doi: 10.1117/12.2080061

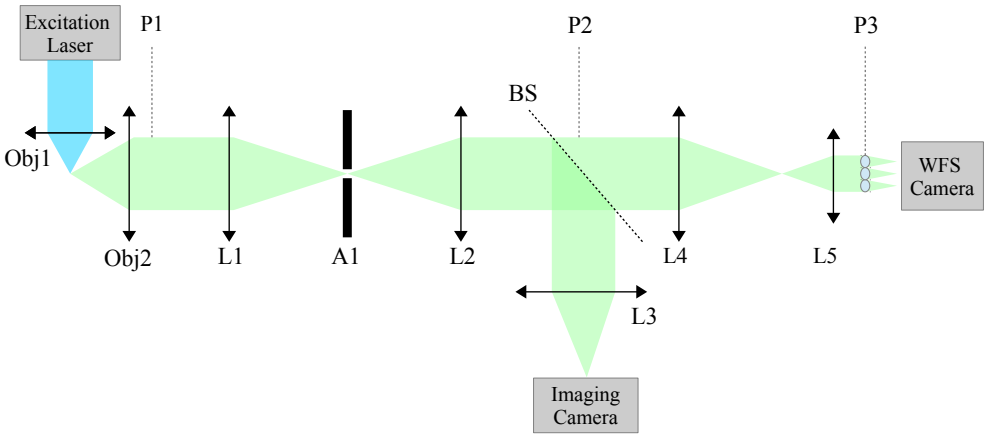

Figure 1. Basic optical setup. The excitation beam (in blue) is orthogonal to the imaging and wavefront sensing beam (in green). Two 4F relays (L1, L2 and L3, L4) reimage and demagnify the imaging objective pupil onto the microlens array, with an aperture (A1) restricting the FoV of the microlenses. The beamsplitter (BS), tube lens (L3) and imaging camera are used to aid in alignment. A brightfield transmission imaging arm and associated illumination is also present, but has been omitted for clarity.

2. EXPERIMENTAL CONFIGURATION

To demonstrate the method we have developed an optical microscope incorporating a Shack Hartmann wavefront sensor and a guide star illumination source where the optical axis of the source beam is orthogonal to the optical axis of the imaging arm, as shown in Figure 1. A collimated 488 nm laser beam is focused into the water filled sample chamber via objective lens OBJ1 (Nikon Plan Fluor 10×, NA 0.3). Fluorescence light emitted by the sample is collected by objective OBJ2 (Nikon CFI LWD 16 × W, NA 0.8). The back aperture of the objective (P1) is re-imaged by a 4F relay (L1, L2) at plane P2, with an aperture (A1) placed in the image plane to limit the field of view of the microlens array. Located at the appropriate distance from P2 is tube lens L3, casting a conventional fluorescence image onto the imaging camera. The plane P2, located in the 50/50 beamsplitter (BS) is demagnified and reimaged onto a microlens array (SMOS Micro-optics, 300 μm pitch, 6 mm focal length) by L4 and L5. Further optics (omitted for clarity) were used to reimage the microlens image plane onto the wavefront sensor (WFS) camera (Andor Zyla 5.5 sCMOS). Also omitted from the diagram for clarity is an IR Köhler illumination system, dichroic beamsplitter and additional imaging camera used to provide transmission brightfield imaging to aid in sample positioning.

The Shack Hartmann wavefront sensor has 12 sub-apertures across its illuminated diameter. Since our guide stars are formed from the structure of the labeled tissue itself, they cannot in general be well approximated as point sources. Therefore, prior to centroiding we cross correlate a reference image (drawn from the central sub-aperture) with every other sub-aperture, thereby obtaining a Gaussian peak shifted in accordance with the local wavefront tilt. This can then be centroided to give the location of the reference image, a technique commonly used in Solar AO[9] and one that has been employed in microscopy.[10] Noise analysis[11] was used to determine the magnitude of non-systematic errors in WFS measurement.

3. CALIBRATION

The null spot positions on the WFS, corresponding to the fixed system aberrations, were measured using a target made by drying 8 μm diameter, volume labeled fluorescent beads (Bangs Labs DG06M) onto the surface of a glass microscope slide. This was then inserted into the sample chamber at an angle to optical axes of both objectives. Because we did not use any bonding agents, relying instead purely on surface adhesion, we could be confident that we had not introduced any further wavefront aberrations, and were able to treat the beads as a definitive guide star for system aberration measurement.

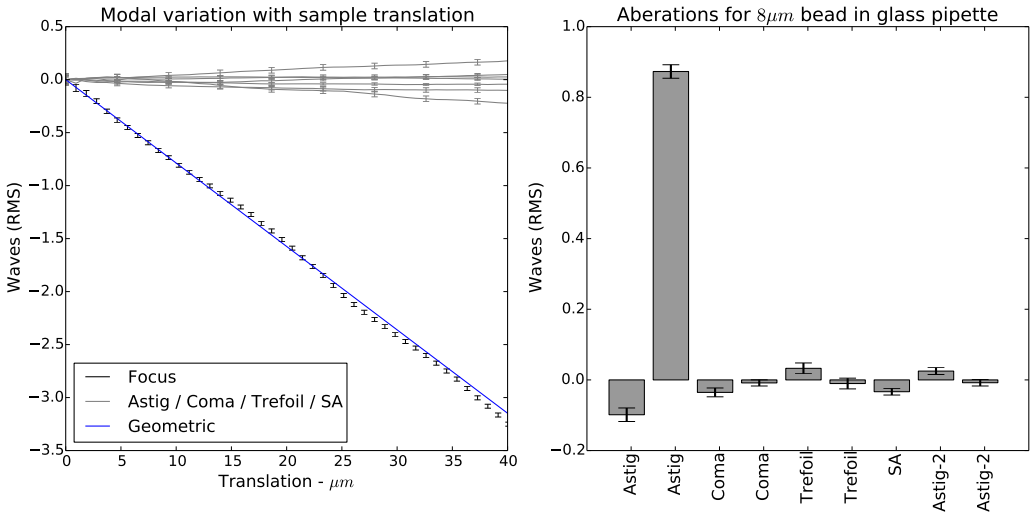

Figure 2. (Left) variations in aberration coefficients as an 8 μm immobilized bead was translated for 40 μm along the axis of the imaging arm (through the excitation beam). (Right) aberrations when imaging an 8 μm bead through a borosilicate glass pipette.

The slide was inserted with a tilt of around 60° relative to the imaging path, to avoid direct laser reflections from the surface which would overwhelm the emission filter and lead to some directly-reflected laser light contaminating the wavefront sensor camera images (we note that this is not a problem when imaging real samples, due to the absence of planar interfaces). Despite the use of a water-filled sample chamber, sufficient beads remained stuck to the slide to allow their use as reference sources.

To verify the WFS calibration, fluorescent beads (as above) were also immobilized within a 0.5 % w/w agarose gel inside a 1.3 mm internal diameter FEP tube. A bead was located near the front of the tube and the WFS spot pattern was recorded under orthogonal illumination. The bead was then translated 40 μm towards the imaging objective with a constant linear velocity. The modal coefficients (with reference to the initial position) for this are shown in Figure 2. As the bead was translated we see a linear change in focus, as expected, and a small quantity of astigmatism as we moved from the optimum focal plane of the objective. Despite a 15-fold decrease in the level of fluorescence over the range of travel due to the inherent depth-sectioning capability of our technique, noise analysis shows that we retain good accuracy, represented as error bars. Also plotted is a geometric prediction of defocus. There is good agreement between the measured wavefront and geometric model up to 15 μm, after which the measured data appears to oscillate slightly; we believe this to be due to minor non-linearity in the constant velocity stage travel.

Further verification was performed using beads immobilized in agar, inside a borosilicate glass pipette (Cole Parmer). The wavefront was measured for a bead near the front of the pipette The primary aberration for the pipette is astigmatism in the axis aligned with the long axis of the pipette. The magnitude is in line with previously presented values measured using sensorless AO and derived from raytracing.[12]

4. RESULTS

Figure 3 shows the time variation of aberrations in the zebrafish heart over a series of successive heartbeats. The aberrations are also shown phase-wrapped to a single beat of the heart. This illustrates the consistency in aberrations between beats, indicating that the instantaneous shapes of the heart throughout its cycle are highly consistent between beats. The positions and number of red blood cells in the heart on successive heartbeats will of course be subject to random variation, but our data implies that this does not have a substantial effect on the measured aberrations. We expect that changing volume of the blood pool inside the heart will have an effect on the aberrations measured when imaging through the heart, but that in the case of low-order aberrations

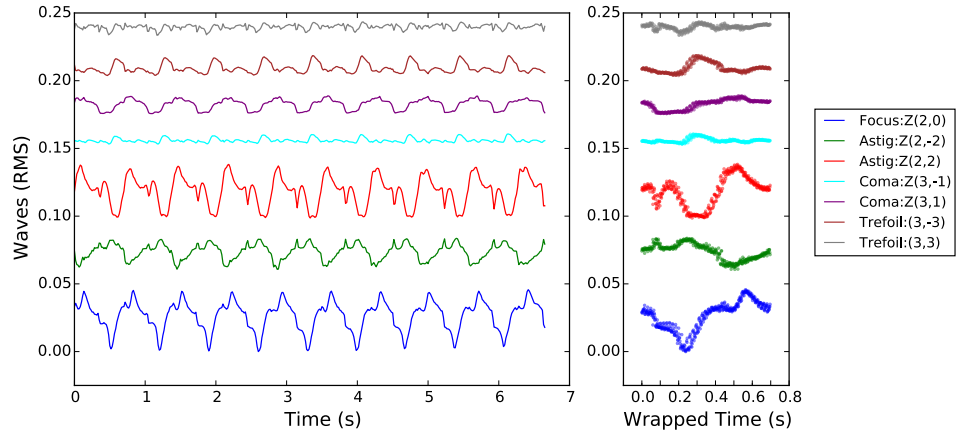

Figure 3. Time-dependent aberrations in the beating heart (near apex of ventricle). Left: aberrations over approximately 8 successive heartbeats; right: aberrations phase-wrapped to show consistency between heartbeats. Modes have been separated vertically relative to their time average aberration value, but the magnitude of the variation is to scale in each case. The modes are labelled according to their corresponding Zernike polynomial.

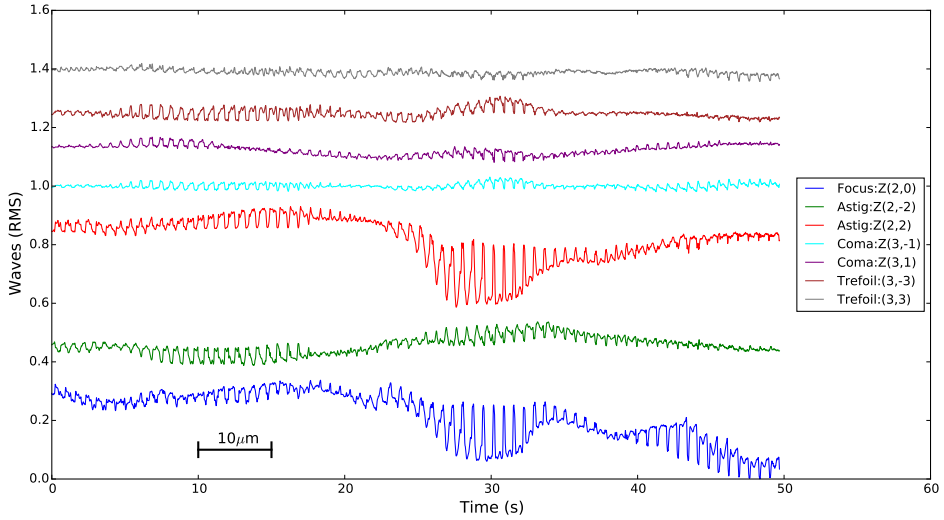

Figure 4. Aberrations measured during a scan in depth through the apex of the beating heart. The curves are a combination of two effects: the increasing depth of imaging within the heart, and the change in aberrations over the course of each heartbeat due to changes in shape of the heart. As in Figure 3, vertical offsets have been applied to the curves for clarity.

its effects can be well described in terms of its mean optical properties, without considering the instantaneous positions of individual blood cells.

Figure 4 shows the changes in aberrations as the imaging plane is scanned down through the heart. The rapid variation is due to changing aberrations over the course of each heartbeat, while the more gradual trend is due to changes with depth in the heart. We note in particular the overall trend of changing defocus with depth. This is a common characteristic of light sheet imaging, especially when imaging a specimen immobilised inside a tube or a cylinder of agarose.[12] The cause of this is a refractive shift of the light sheet relative to the focal plane of the imaging objective, although certain imaging configurations[13] could have the potential to correct for this error through dynamic refocusing of the imaging objective during a z scan.

5. CONCLUSION

We have demonstrated a novel method of generating a laser guide star using the intrinsic fluorescence of a living biological specimen. The technique is suitable for use in regions consisting of fluorescently labelled linear structures (e.g. blood vessels) or 2D surfaces (e.g. heart wall, epidermis). By combining an orthogonally-launched excitation laser with a iris in the image plane, we are able to eliminate background light and provide localization in all three dimensions without filtering the wavefront. This allows us to perform snapshot measurements of tissue aberrations in a bulk living specimen.

We have shown that such laser guide stars can be used for wavefront sensing. In addition to being a means of surveying aberration levels in different regions of a specimen, an important application of this is wavefront correction for AO microscopy. We note that our technique is particularly well-suited to an automated AO scheme if the imaging system is based around a DSLM light sheet microscope,[14] a design in which the light sheet is formed by rapid vertical scanning of a focused Gaussian beam. In this configuration it would be possible to temporarily pause the scanning of the beam, with the beam illuminating a suitable target region of fluorescence. The wavefront could then be measured and adaptively corrected, before scanning was resumed to allow widefield image acquisition. Such a scheme is inspired by the procedure described by Tao *et al*,[8] but would have additional flexibility from our ability to generate 3D localized guide stars in a wide range of biological tissues.

APPENDIX

Here we will consider the size of the iris in the image plane, and its effect on aberration measurements. We will calculate the size of the pinhole needed to provide depth discrimination in a conventional z-illuminated guide star system, and give a simpler analysis for larger aberrations than that presented by Shaw *et al.*[15]

Suppose we need a depth discrimination represented by a depth range d in the sample. Assuming geometrical optics the beam size at a distance d from the focus is given by s, where

$$s = 2d \tan\left(\sin^{-1}\left(\frac{\mathrm{NA}}{n}\right)\right)$$

and where NA is the numerical aperture and n the refractive index of the sample. The confocal pinhole can only filter out a portion of this light (never 100 %). If we assume an extinction factor of e_x (where 0 is full extinction and 1 is no extinction) then the pinhole size, s_{confocal}, needs to be:

$$s_{\mathrm{confocal}} = \sqrt{e_x s^2} \tag{1}$$

Next consider the size of the pinhole such that the beam is not spatially filtered. This will depend on the magnitude and type of the aberrations – for larger and more complex aberrations we will require a larger pinhole to avoid filtering them. The minimum resolvable feature size in a diffraction limited microscope is given in the Rayleigh limit (from the peak of the PSF to the first minimum) as $\lambda/2\mathrm{NA}$, where λ is the wavelength of light. Therefore the pinhole diameter should be double this to enable all of the central portion of the PSF to pass. When the beam is aberrated then this will need to be increased. Consider the simplest case of tip-tilt aberration and restrict the required tip-tilt to be ± 1 wave, in which case a further doubling of the pinhole size is needed to $2\lambda/\mathrm{NA}$. We can now scale this argument up to higher order aberrations and note that the wavefront sensor sub-aperture size in an AO system needs to be matched to the aberrations (or at least the ones to be corrected) and that therefore the pinhole size needed so as not to spatial filter the wavefront is given by s_{sf} where

$$s_{sf} = \frac{2\lambda N_{SH}}{\mathrm{NA}} \tag{2}$$

and where N_{SH} is the number of Shack Hartman sub-apertures across the beam. The optimum pinhole size – where confocal depth rejection is balanced against spatial filtering – can then be defined by equating equations 1 and 2, and rearranging to define a maximum number of Shack Hartmann sub-apertures above which sensing and correction will not occur (i.e. higher spatial order aberrations will not be sensed),

$$N_{SH} = \frac{\sqrt{e_x} b \mathrm{NA}}{\lambda} \tan\left(\sin^{-1}\left(\frac{\mathrm{NA}}{n}\right)\right)$$

An approximate value for d can be chosen as the average distance between structures or "blobs in the specimen. since the purpose of the pinhole filtering is to reject light from out-of-focus structures. Using some typical values of NA=0.6, n=1.33, λ=550 nm, e_x=0.1 gives $N_{SH} = 2$ for d=10 μm, which is clearly too small for anything but tip-tilt correction. If we wish to make a high order AO system with, say, $N_{SH} = 20$ then the spacing between structures needs to be around 100 μm – which is much too large for many specimens. This clearly shows the problem of using a z-illuminated guide star where we need either to have only a very low order AO system (with small aberrations) or have an unreasonably sparse biological specimen.

In contrast, in our technique no spatial filtering is required. Although a (comparatively wide) aperture is present, this lies in a conjugate image plane and hence does not spatially filter the wavefront. The sole purpose of the aperture is to restrict the field of view of the wavefront sensor, and its presence does not alter the modes sensed by the wavefront sensor.

ACKNOWLEDGMENTS

The authors acknowledge funding from the UK Engineering and Physical Sciences Research Council (grant ref EP/I010173/1), which supported the preliminary work on this topic.

REFERENCES

[1] Booth, M. J., "Adaptive optics in microscopy.," *Philosophical transactions. Series A, Mathematical, physical, and engineering sciences* **365**, 2829–43 (Dec. 2007).

[2] Girkin, J. M., Poland, S., and Wright, A. J., "Adaptive optics for deeper imaging of biological samples," *Current opinion in biotechnology* **20**, 106–110 (2009).

[3] Gould, T. J., Burke, D., Bewersdorf, J., and Booth, M. J., "No TitleAdaptive optics enables 3D STED microscopy in aberrating specimens," *Optics Express* **20**, 20998–21009 (2012).

[4] Débarre, D., Botcherby, E. J., Watanabe, T., Srinivas, S., Booth, M. J., and Wilson, T., "Image-based adaptive optics for two-photon microscopy," *Optics Letters* **34**(16), 2495–2497 (2009).

[5] Bourgenot, C., Taylor, J. M., Saunter, C. D., Girkin, J. M., and Love, G. D., "Light sheet adaptive optics microscope for 3D live imaging," *Proc. SPIE* **8589**, 85890W (Feb. 2013).

[6] Roddier, F., [*Adaptive Optics in Astronomy*], Cambridge University Press (2004).

[7] Tao, X., Fernandez, B., Azucena, O., Fu, M., Garcia, D., Zuo, Y., Chen, D. C., and Kubby, J., "Adaptive optics confocal microscopy using direct wavefront sensing.," *Optics letters* **36**, 1062–4 (Apr. 2011).

[8] Tao, X., Crest, J., Kotadia, S., Azucena, O., Chen, D. C., Sullivan, W., and Kubby, J., "Live imaging using adaptive optics with fluorescent protein guide-stars," *Optics Express* **20**(14), 3389–3391 (2012).

[9] Löfdahl, M. G., "Astrophysics Evaluation of image-shift measurement algorithms for solar Shack-Hartmann wavefront sensors," *Astronomy & Astrophysics* **524**, A90 (2010).

[10] Bourgenot, C., *Light sheet adaptive optics microscope for 3D live imaging*, PhD thesis, Durham University (2013).

[11] Saunter, C. D., "Quantifying subpixel accuracy: an experimental method for measuring accuracy in image-correlation-based, single-particle tracking.," *Biophysical journal* **98**, 1566–70 (Apr. 2010).

[12] Bourgenot, C., Saunter, C. D., Taylor, J. M., Girkin, J. M., and Love, G. D., "3D adaptive optics in a light sheet microscope.," *Optics express* **20**, 13252–61 (June 2012).

[13] Fahrbach, F. O., Voigt, F. F., Schmid, B., Helmchen, F., and Huisken, J., "Rapid 3D light-sheet microscopy with a tunable lens," *Optics Express* **21**(18), 21010–21026 (2013).

[14] Keller, P. J., Schmidt, A. D., Wittbrodt, J., and Stelzer, E. H. K., "Digital scanned laser light-sheet fluorescence microscopy (DSLM) of zebrafish and Drosophila embryonic development.," *Cold Spring Harbor Protocols* **2011**, 1235–43 (Oct. 2011).

[15] Shaw, M., O'Holleran, K., and Paterson, C., "Investigation of the confocal wavefront sensor and its application to biological microscopy.," *Optics express* **21**, 19353–62 (Aug. 2013).